possible applications of the PSCOF technology to nonliquid crystalline areas. This technology should permit one to prepare sandwiches of LCs between polymer films and vice versa and self-supporting thin and flexible displays. Fabrication of multilayer structures perpendicular to the substrate, for use in switchable gratings and other diffractive optics applications, is possible with the use of masks during phase separation. Electrically controllable LC microlenses, two-dimensional optical gratings, and other microstructures have been prepared with the PSCOF method.

References and Notes

1. P. S. Drzaic, Ed., *Liquid Crystal Dispersions* (World Scientific, Singapore, 1995).
2. G. Crawford and S. Zumer, Eds., *Liquid Crystals in Complex Geometries* (Taylor & Francis, London, 1996).
3. J. W. Doane, N. A. Vaz, B.-G. Wu, S. Zumer, *Appl. Phys. Lett.* **48**, 269 (1986).
4. L. Blinov and V. Chigrinov, *Electrooptical Effects in Liquid Crystals* (Springer-Verlag, New York, 1993).
5. N. A. Clark, T. Rieker, J. Maclennanl, *Ferroelectrics* **85**, 79 (1988).
6. V. Krongauz, E. Schmelzer, R. Yohannan, *Polymer* **32**, 1654 (1991).
7. N. A. Clark and S. T. Lagerwall, *Appl. Phys. Lett.* **36**, 899 (1980).
8. V. Vorflusev and S. Kumar, *Ferroelectrics* **213**, 117 (1998).
9. A. Fukuda, Y. Takanishi, T. Isozaki, K. Ishikawa, H. Takezoe, *J. Mater. Chem.* **4**, 997 (1994).

10. Supported in part by NSF Science and Technology Center ALCOM grant DMR-89-20147.

12 November 1998; accepted 5 February 1999

An Adiabatic Quantum Electron Pump

M. Switkes,[1] C. M. Marcus,[1*] K. Campman,[2] A. C. Gossard[2]

A quantum pumping mechanism that produces dc current or voltage in response to a cyclic deformation of the confining potential in an open quantum dot is reported. The voltage produced at zero current bias is sinusoidal in the phase difference between the two ac voltages deforming the potential and shows random fluctuations in amplitude and direction with small changes in external parameters such as magnetic field. The amplitude of the pumping response increases linearly with the frequency of the deformation. Dependencies of pumping on the strength of the deformations, temperature, and breaking of time-reversal symmetry were also investigated.

Over the past decade, research into the electrical transport properties of mesoscopic systems has provided insight into the quantum mechanics of interacting electrons, the link between quantum mechanics and classical chaos, and the decoherence responsible for the transition from quantum to classical physics (*1, 2*). Most of this research has focused on transport driven directly by an externally applied bias. We present measurements of an adiabatic quantum electron pump, exploring a class of transport in which the flow of electrons is driven by cyclic changes in the wave function of a mesoscopic system.

A deformation of the confining potential of a mesoscopic system that is slow compared with the relevant energy relaxation times changes the wave function of the system while maintaining an equilibrium distribution of electron energies. In systems connected to bulk electron reservoirs by open leads supporting one or more transverse quantum modes, the wave function extends into the leads and these adiabatic changes can transport charge to or from the reservoirs. A periodic deformation that depends on a single parameter cannot result in net transport; any charge that flows during the first half-period will flow back during the second. On the other hand, deformations that depend on two or more parameters changing in a cyclic fashion can break this symmetry and, in general, can provide net transport. This transport mechanism was originally described by Thouless (*3*) for isolated (or otherwise gapped) systems at zero temperature. The theory has been extended to open systems at finite temperature (*4–6*). Here, we present an experimental investigation of this phenomenon.

Before we characterize the adiabatic quantum pump in the present experiment, it is useful to recall other mechanisms that produce a dc response to an ac driving signal in coherent electronic systems. One mechanism relies on absorption of radiation to create a nonequilibrium distribution of electron energies, which leads to photon-assisted tunneling (*7*) in systems with asymmetric tunneling leads and a mesoscopic photovoltaic effect (*8*) in open systems. A second mechanism, the classical analog of the quantum pumping measured in this experiment, has been observed in single (*9*) and multiple (*10*) quantum dots in which transport is dominated by the Coulomb blockade (*2*). In this regime, the capacitive energy needed to add a single electron to the system is greater than the temperature and applied bias, blockading transport through the dot. Electrons can be added one by one by changing the potential of the isolated dot relative to the reservoirs. Each cycle begins by isolating the system from one electron reservoir—for example, by increasing the height of one tunneling barrier—while forcing one or more electrons to enter from the other reservoir by changing the potential in the system. The cycle is continued by reversing the configuration to isolate the system from the reservoir that supplied the electrons and forcing the extra electrons out into the other reservoir, yielding a net flow quantized in units of the electron charge times the frequency applied. This cycle requires two ac control voltages with a phase difference between them. The magnitude and direction of the pumping are determined by these voltages; there are no random fluctuations due to quantum effects. The control and quantization of current provided by the Coulomb blockade pump has motivated its development for use as a precision current standard [see, for example, (*11*)].

Adiabatic quantum pumping in open structures also requires two ac voltages and produces a response that is linear in the ac frequency. However, because the system is open to the reservoirs, Coulomb blockade is absent and the pumping response is not quantized. Quantum pumping is driven not by cyclic changes to barriers and potentials, but by shape changes in the confining potential or other parameters that affect the interference pattern of the coherent electrons in the device.

Many aspects of adiabatic quantum pumping can be understood in terms of the emissivity, dn/dX, which characterizes the number of electrons n entering or leaving the device in response to a small change in some parameter δX, such as a distortion of the confining potential (*12*). The change in the charge of the dot is thus $\delta Q = e\Sigma\delta X_i dn/dX_i$. Integrating along the closed path in the i-dimensional space of parameters X_i defined by the pumping cycle then yields the total charge pumped during each cycle (*6*). For the particular case of pumping with two parameters (for example, shape distortions at two locations on the dot), the line integral can be written as an integral over the surface enclosed by the path, $Q \propto \int_\alpha \xi dX_1 dX_2$ (*6*), where ξ depends on the emissivities at points in parameter space enclosed by the path. Because changes in external parameters rearrange the electron interference pattern in the device, emissivities fluctuate randomly as parameters are changed, similar to the well-known mesoscopic fluctuations of conductance in coherent samples.

[1]Department of Physics, Stanford University, Stanford, CA 94305, USA. [2]Materials Department, University of California, Santa Barbara, CA 93106, USA.

*To whom correspondence should be addressed. E-mail: cmarcus@stanford.edu

When the pumping parameters vary by less than the correlation length of the fluctuations of emissivity, ξ remains essentially constant throughout the pumping cycle and the total charge pumped per cycle depends only on the area enclosed by the path in parameter space, α. These straightforward observations explain many of the qualitative features of our data.

We made measurements of adiabatic quantum pumping in three similar semiconductor quantum dots defined by electrostatic gates patterned on the surface of a GaAs-AlGaAs heterostructure using standard electron-beam lithography techniques. Negative voltages (~ -1 V) applied to the gates formed the dot by depleting the two-dimensional electron gas at the heterointerface 56 nm (device 1) or 80 nm (devices 2 and 3) below the surface. All three dots had lithographic areas $a_{\rm dot} \sim 0.5\ \mu\text{m}^2$, giving an average single particle level spacing $\Delta = 2\pi\hbar^2/m^* a_{\rm dot} \sim 13\ \mu$V ($\approx$150 mK), where $\hbar$ is Planck's constant (h) divided by 2π and m^* is the effective electron mass. The three devices showed similar behavior, and most of the data presented here are for device 3. In the micrograph of device 1 (Fig. 1C), the three gates marked with red circles control the conductances of the point-contact leads that connect the dot to electronic reservoirs. Voltages on these gates were adjusted so that each lead transmitted $N \sim 2$ transverse modes, giving an average conductance through the dot $g \sim 2e^2/h$. The remaining two gates were used to create both periodic shape distortions necessary for pumping and static shape distortions that allow ensemble averaging (*13, 14*).

Except where noted, measurements were made at a pumping frequency $f = 10$ MHz, base temperature $T = 330$ mK, dot conductance $g \sim 2e^2/h \approx (13\ \text{kilohm})^{-1}$, and ac gate voltage $A_{\rm ac} = 80$ mV peak-to-peak. For comparison, the gate voltage necessary to change the electron number in the dot by one is $\sim$5 mV. Measurements were carried out over a range of magnetic field, B, from 30 to 80 mT, which allows several quanta of magnetic flux, $\varphi_0 = h/e$, to penetrate the dot ($\varphi_0/a_{\rm dot} \sim$ 10 mT) while keeping the classical cyclotron radius much larger than the dot size ($r_{\rm cyc}$[μm] $\sim 80/B$[mT]).

The general characteristics of quantum pumping, including antisymmetry about phase difference $\phi = \pi$, sinusoidal dependence on ϕ (for small amplitude pumping), and random fluctuations of amplitude as a function of perpendicular magnetic field, are illustrated in Fig. 1. The pumping amplitude is quantified by the values A_0 and B_0, which are extracted from fits of the form $V_{\rm dot}(\phi) = A_0 \sin\phi + B_0$ (shown as dotted lines in Fig. 1B).

Because pumping fluctuations extend on both sides of zero (pumping occurs in either direction) with equal likelihood for a given ϕ, $\langle A_0 \rangle$ is small and the pumping amplitude is instead characterized by $\sigma(A_0)$, the standard deviation of A_0. For example, the data in Fig. 2B yield $\langle A_0 \rangle = 0.01\ \mu$V and the standard deviation $\sigma(A_0) = 0.4\ \mu$V. Values of $\sigma(A_0)$ (Figs. 2, 3, and 4) are based on 96 independent configurations over B, $V_{\rm g1}$, and $V_{\rm g2}$ (Fig. 2B).

The dependence of the pumping amplitude $\sigma(A_0)$ on pumping frequency is linear (Fig. 2). For the above parameters, the linear dependence has a slope of 40 nV/MHz. Because the dot has conductance $g \sim 2e^2/h$, this voltage compensates a pumped current of 3 pA/MHz, or about 20 electrons per pump cycle. The dependence of $\sigma(A_0)$ on the pumping strength $A_{\rm ac}$ (Fig. 3) shows that for weak pumping, $A_{\rm ac} < 80$ mV, $\sigma(A_0)$ is proportional to $A_{\rm ac}^2$, as expected from the simple loop-area argument described above. For stronger pumping, $\sigma(A_0)$ increases more slowly than $A_{\rm ac}^2$, with a crossover from weak to strong

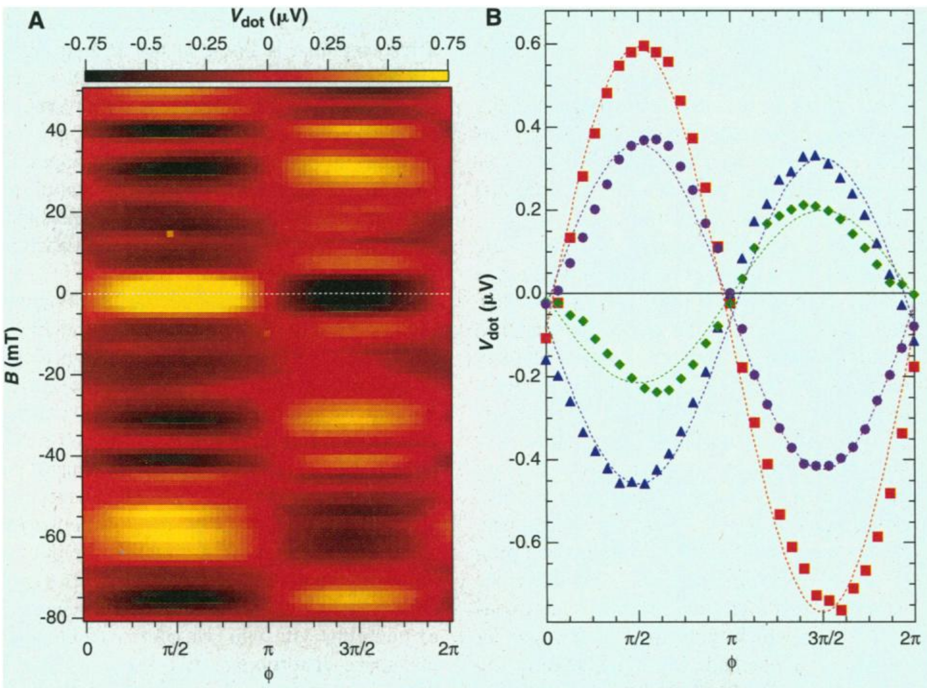

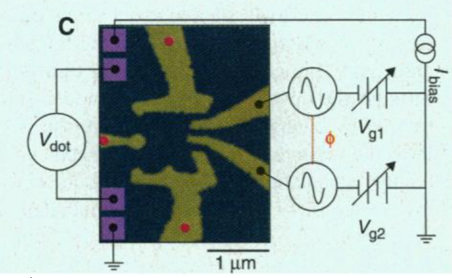

Fig. 1. (A) Pumped dc voltage $V_{\rm dot}$ as a function of the phase difference ϕ between two shape-distorting ac voltages and magnetic field B. Note the sinusoidal dependence on ϕ and the symmetry about $B = 0$ (dashed white line). (B) Plot of $V_{\rm dot}(\phi)$ for several different magnetic fields (solid symbols) along with fits of the form $V_{\rm dot} = A_0 \sin\phi + B_0$ (dashed curves). (C) Schematic of the measurement set-up and micrograph of device 1. The bias current is set to 0 for pumping measurements.

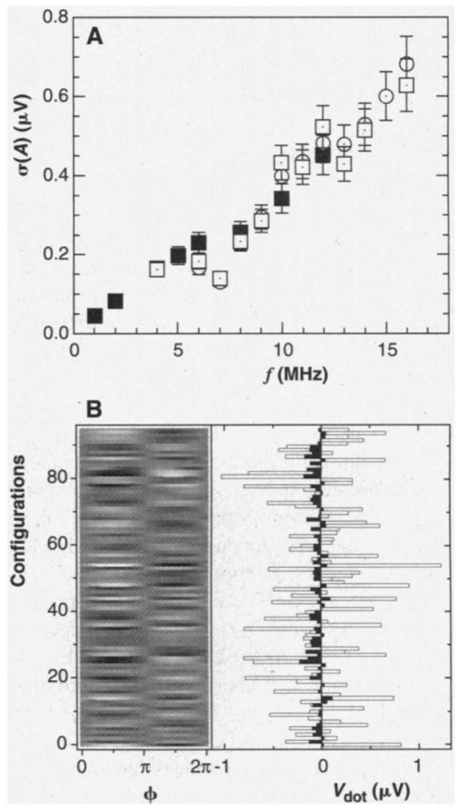

Fig. 2. (A) Standard deviation of the pumping amplitude, $\sigma(A_0)$, as a function of ac pumping frequency. The slope is $\sim$40 nV/MHz for both device 2 (solid symbols) and 3 (open symbols). Circular symbols represent a second set of data taken for device 3. (B) A typical data set corresponding to one point in (A), along with fit parameters A_0 (open bars) and B_0 (solid bars) for each configuration.

pumping occurring near the characteristic gate voltage scale of fluctuations in both dot conductance and pumping, measured independently to be 70 ± 6 mV. This departure from an A_{ac}^2 dependence for strong pumping is expected to occur when the loop in parameter space that describes the pumping cycle becomes sufficiently large that it encloses uncorrelated emissivities (*5, 6*). In this case, one would expect $\sigma(A_0) \propto A_{ac}$, neglecting any correlations. However, the observed dependence at strong pumping is slower than linear, and in fact appears consistent with $\sigma(A_0) \propto A_{ac}^{1/2}$. This unexpectedly slow dependence may result if significant heating and dephasing of electrons occurs as a result of strong pumping. Further study is needed to investigate this. Another characteristic of strong pumping is that $V_{dot}(\phi)$ becomes nonsinusoidal, as seen in the lower inset of Fig. 3. Notice that $V_{dot}(\phi = \pi)$ remains close to zero for all pumping strengths whereas $V_{dot}(\phi = 0)$ deviates from 0 at strong pumping.

The temperature dependence of $\sigma(A_0)$ for pumping strength near the crossover from weak to strong pumping, A_{ac} = 80 mV, is shown in Fig. 4. At high temperatures (1 to 5.5 K), $\sigma(A_0)$ is well described by a power law, $\sigma(A_0) = 0.2T^{-0.9}$ [for $\sigma(A_0)$ in microvolts and T in kelvin]. This behavior presumably reflects the combined influence of thermal smearing, which alone is expected to yield $\sigma(A_0) \propto T^{-1/2}$, and temperature-dependent dephasing. A similar temperature dependence is found for the amplitude of conductance fluctuations in dots (*15*). Below 1 K, the temperature dependence begins to round off, perhaps indicating a saturation at lower temperatures. A low-temperature saturation of pumping is expected when thermal smearing becomes less than lifetime broadening (*16*), $k_B T < [\Gamma_{esc} + \Gamma_\varphi(T)]$, where k_B is the Boltzmann constant, $\Gamma_{esc} = N\Delta/\pi$ (N is the number of modes per lead) is the broadening due to escape through the leads, and $\Gamma_\varphi(T)$ is the broadening due to dephasing, $\Gamma_\varphi(T) = \hbar/\tau_\varphi$. Using $N \sim 2$ and known dephasing times τ_φ in similar dots (*15*) yields an expected saturation at ~100 mK, consistent with the rounding seen in the data.

Finally, we investigated the symmetries and statistical properties of adiabatic quantum pumping. The symmetry of pumping fluctuations about zero magnetic field is seen in the gray-scale plot of $V_{dot}(\phi = \pi/2)$ as a function of B and the dc voltage on one shape-distorting gate, V_{g1} (Fig. 5A). The full symmetry of pumping follows from time-reversal symmetry: $V_{dot}(\phi, B) = -V_{dot}(-\phi, -B)$, analogous to the Landauer-Büttiker relations for conductance (*5*). The reduced symmetry observed in Fig. 5A, $V_{dot}(\phi, B) = V_{dot}(\phi, -B)$, results from a combination of time-reversal symmetry and the symmetry $V_{dot}(\phi, B) = -V_{dot}(-\phi, B)$ implied by the sinusoidal dependence of V_{dot} on ϕ at low pumping amplitudes.

A central paradigm in mesoscopic physics is that the statistical properties of a fluctuating quantity depend on the symmetries of the system and little else. To investigate how the statistics of pumping fluctuations depend on time-reversal symmetry, we measured $V_{dot}(\phi = \pi/2)$, as well as the conductance, as a function of magnetic field for 36 independent configurations of V_{g1} and V_{g2}. The sampling in B is much finer than the characteristic magnetic field scales for pumping fluctuations (3.3 ± 0.4 mT) and conductance fluctuations (3.9 ± 0.4 mT), where these values are the half-maxima of the autocorrelations of the fluctuations. These values are comparable to and somewhat smaller than one flux quantum through the device, consistent with theory and previous experiments on conductance in similar dots (*17*). The average pumped voltage, $\langle V_{dot}(\phi = \pi/2)\rangle$, is close to zero and has no outstanding features other than its symmetry in magnetic field. On the other hand, $\sigma[V_{dot}(\phi = \pi/2)]$ shows a peak at $B = 0$ of about twice its value away from zero field. The peak width is comparable to the correlation field (Fig. 5B), suggesting that the peak is associated with the breaking of time-reversal symmetry. We conclude that pumping fluctuations are larger for the time-reversal symmetric case at $B = 0$, similar to the situation for conductance fluctuations (*13*).

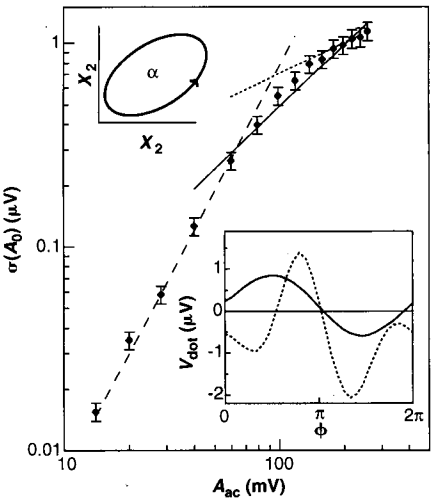

Fig. 3. Standard deviation of the pumping amplitude, $\sigma(A_0)$, as a function of the ac driving amplitude A_{ac}, along with fits to $\sigma(A_0) \propto A_{ac}^2$ below 80 mV (dashed line), $\sigma(A_0) \propto A_{ac}$ (solid line), and $\sigma(A_0) \propto A_{ac}^{1/2}$ (dotted line) above 80 mV. The lower inset shows that the sinusoidal dependence of $V_{dot}(\phi)$ at small and intermediate values of A_{ac} (solid curve, A_{ac} = 100 mV) becomes nonsinusoidal for strong pumping (dotted curve, A_{ac} = 260 mV), but maintains $V_{dot}(\pi) = 0$, as required by time-reversal symmetry. The upper inset is a schematic of the loop swept out by the pumping parameters X_1 and X_2. The charged pumped per cycle can be written in terms of an integral over the surface α enclosed by the loop.

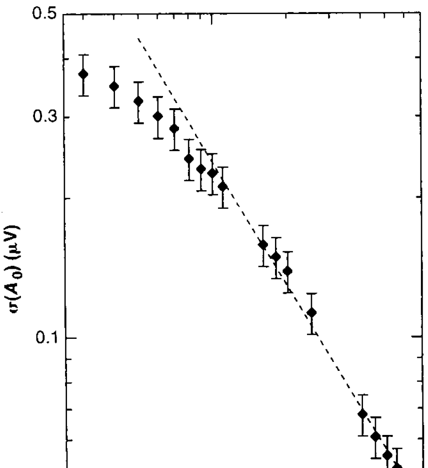

Fig. 4. Pumping amplitude $\sigma(A_0)$ as a function of temperature T with a power law fit (dashed line). At lower temperatures, there is a rounding off of the T dependence, consistent with an expected saturation when lifetime broadening exceeds temperature below ~100 mK.

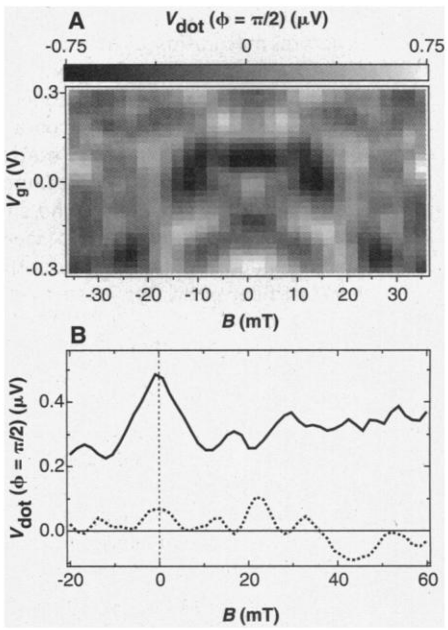

Fig. 5. (**A**) Gray-scale plot of $V_{dot}(\phi = \pi/2)$ as a function of magnetic field B and dc gate voltage V_{g1} (*18*). Note the symmetry and the characteristic scales of pumping fluctuations. (**B**) Average (dotted curve) and standard deviation (solid curve) of 36 uncorrelated samples of $V_{dot}(\phi = \pi/2)$ as a function of B measured at different dc gate voltages, V_{g1} and V_{g2} [not the same data set as (A)]. The average is small and fluctuates around zero. The standard deviation shows a peak around $B = 0$ about twice its value away from zero with a width corresponding to about one quantum of flux, h/e, through the dot.

References and Notes

1. C. W. J. Beenakker and H. Van Houten, in *Solid State Physics*, H. Ehrenreich and D. Turnbull, Eds. (Academic Press, San Diego, CA, 1991), vol. 44, pp. 1–228.
2. L. P. Kouwenhoven *et al.*, in *Proceedings of the Advanced Study Institute on Mesoscopic Electron Transport*, L. P. Kouwenhoven, G. Schön, L. L. Sohn, Eds. (Kluwer, Dordrecht, 1997), series E.
3. D. J. Thouless, *Phys. Rev. B* **27**, 6083 (1983).
4. B. Spivak, F. Zhou, M. T. Beal Monod, *ibid.* **51**, 13226 (1995).
5. F. Zhou, B. Spivak, B. L. Altshuler, *Phys. Rev. Lett.* **82**, 608 (1999).
6. P. W. Brouwer, *Phys. Rev. B* **58**, 10135 (1998).
7. L. P. Kouwenhoven *et al.*, *ibid.* **50**, 2019 (1994); L. P. Kouwenhoven *et al.*, *Phys. Rev. Lett.* **73**, 3443 (1994).
8. V. I. Fal'ko and D. E. Khmel'nitskiĭ, *Zh. Eksp. Teor. Fiz.* **95**, 328 (1989) [*Sov. Phys. JTEP* **68**, 186 (1989)]; J. Liu, M. A. Pennington, N. Giordano, *Phys. Rev. B* **45**, 1267 (1992).
9. L. P. Kouwenhoven, A. T. Johnson, N. C. van der Vaart, C. J. P. M. Harmans, C. T. Foxon, *Phys. Rev. Lett.* **67**, 1626 (1991); L. P. Kouwenhoven *et al.*, *Z. Phys. B* **85**, 381 (1991).
10. H. Pothier, P. Lafarge, C. Urbina, D. Esteve, M. H. Devoret, *Europhys. Lett.* **17**, 249 (1992).
11. M. W. Keller, J. M. Martinis, R. L. Kautz, *Phys. Rev. Lett.* **80**, 4530 (1998).
12. M. Büttiker, H. Thomas, A. Prêtre, *Z. Phys. B* **94**, 133 (1994).
13. H. U. Baranger and P. A. Mello, *Phys. Rev. Lett.* **73**, 142 (1994); R. A. Jalabert, J.-L. Pichard, C. W. J. Beenakker, *Europhys. Lett.* **27**, 255 (1994); I. H. Chan, R. M. Clarke, C. M. Marcus, K. Campman, A. C. Gossard, *Phys. Rev. Lett.* **74**, 3876 (1995).
14. Voltages on these gates have a dc component, V_g, and an ac component (at megahertz frequencies) produced by two frequency-locked synthesizers (HP 3325) with a computer-controlled phase difference ϕ between them. To allow a sensitive lock-in measurement of the pumping signal, the ac gate voltages are chopped by a low-frequency (93 Hz) square wave, and the voltage across the dot is measured synchronously with a PAR 124 lock-in amplifier. A bias current can also be applied directly from the lock-in amplifier, allowing conductance to be measured without disturbing the measurement set-up. The current bias is then set to zero to measure pumping.
15. A. G. Huibers, M. Switkes, C. M. Marcus, K. Campman, A. C. Gossard, *Phys. Rev. Lett.* **81**, 1917 (1998).
16. F. Zhou, personal communication.
17. C. M. Marcus *et al.*, *Chaos Solitons Fractals* **8**, 1261 (1997).
18. The line of symmetry is slightly shifted from the "$B = 0$" line determined from the magnet current as a result of offset magnetic fields.
19. We thank B. Altshuler, A. Auerbach, P. Brouwer, A. Morpurgo, B. Spivak, and F. Zhou for useful discussions. We acknowledge support at Stanford from the Army Research Office under contract DAAH04-95-1-0331 and the NSF-Presidential Faculty Fellowship under contract DMR-9629180-1, and at University of California, Santa Barbara, from the Air Force Office of Scientific Research under grant number F49620-94-1-0158 and by QUEST, an NSF Science and Technology Center.

22 October 1998; accepted 6 January 1999

Structural Maturation of Neural Pathways in Children and Adolescents: In Vivo Study

Tomáš Paus,*[1] Alex Zijdenbos,[1] Keith Worsley,[1] D. Louis Collins,[1] Jonathan Blumenthal,[2] Jay N. Giedd,[2] Judith L. Rapoport,[2] Alan C. Evans[1]

Structural maturation of fiber tracts in the human brain, including an increase in the diameter and myelination of axons, may play a role in cognitive development during childhood and adolescence. A computational analysis of structural magnetic resonance images obtained in 111 children and adolescents revealed age-related increases in white matter density in fiber tracts constituting putative corticospinal and frontotemporal pathways. The maturation of the corticospinal tract was bilateral, whereas that of the frontotemporal pathway was found predominantly in the left (speech-dominant) hemisphere. These findings provide evidence for a gradual maturation, during late childhood and adolescence, of fiber pathways presumably supporting motor and speech functions.

Structural maturation of individual brain regions and their connecting pathways is a condition *sine qua non* for the successful development of cognitive, motor, and sensory functions. The smooth flow of neural impulses throughout the brain allows for information to be integrated across the many spatially segregated brain regions involved in these functions. The speed of neural transmission depends not only on the synapse, but also on structural properties of the connecting fibers, including the axon diameter and the thickness of the insulating myelin sheath (*1*). Axons constituting major fiber pathways in the human brain, such as those of the corpus callosum or the corticospinal tract, continue to develop throughout childhood and adolescence. Postmortem studies suggest that axon diameter and myelin sheath undergo conspicuous growth during the first 2 years of life, but may not be fully mature before adolescence (*2*) or even late adulthood (*3*). However, the scarcity of brain specimens makes it difficult to draw definite conclusions about the timetable of myelination during childhood and adolescence. In vivo studies with magnetic resonance imaging (MRI) therefore play a major role in filling this gap. Previous developmental MRI studies have provided evidence for a continuous increase in the overall volume of white matter and the area of the corpus callosum well into adolescence (*4*), but the analytic procedures used in these studies did not allow the investigators to detect changes in specific corticocortical or corticofugal white matter pathways. Here, we report findings obtained with a technique for computational analysis of age-related changes in local white matter signal throughout the brain. Similar techniques have been used in adults to detect subtle regional differences in gray matter signal between healthy subjects and patients with psychiatric or neurological disorders (*5, 6*).

[1]Montreal Neurological Institute, McGill University, 3801 University Street, Montreal, Quebec H3A 2B4, Canada. [2]Child Psychiatry Branch, National Institute of Mental Health, Building 10, Room 6N240, 10 Center Drive, MSC-1600, Bethesda, MD 20892, USA.

*To whom correspondence should be addressed. E-mail: tomas@bic.mni.mcgill.ca

We obtained brain MRI scans of 111 children and adolescents aged 4 to 17 years (*7*). The images were then processed in a fully automatic system that included the following steps: (i) nonlinear transformation of images into standardized stereotactic space to remove global and local differences in the size and shape of the individual brains; (ii) classification of brain tissue into white matter, gray matter, and cerebrospinal fluid; and (iii) blurring of white matter binary masks to generate three-dimensional (3D) maps of white matter "density" (*8*). Using a linear regression model, we correlated the 111 individual maps of white matter density with the subject's age on a voxel-by-voxel basis (*9*).

Regression analysis revealed significant ($t > 5.0$, $P < 0.04$, corrected) age-related increases in white matter density within the left ($t = 8.9$, $r = 0.65$) and right ($t = 8.0$, $r = 0.60$) internal capsule (Fig. 1) and the posterior portion of the left arcuate fasciculus ($t = 6.6$, $r = 0.54$; Fig. 2). The location of the changes in the posterior limb of the internal capsule suggested that the changes involved the corticospinal and, possibly, thalamocortical tracts. Changes in white matter density within the internal capsule were small but consistent, increasing linearly from age 4 to age 17 by about two standard deviations (Fig. 3). The arcuate fasciculus contains fibers connecting frontal and temporal cortical regions involved in speech. It is therefore noteworthy that age-related white matter increases in this pathway reached significance only in the left but not the right hemisphere; the left hemisphere can be assumed to be dominant for speech in the majority of our right-handed subjects (*10*). The mean white matter density